Iranian Journal of Chemical Engineering
Vol. 13, No. 4 (Autumn 2016), IAChE

Three-dimensional CFD Modeling of Fluid Flow and Heat Transfer Characteristics of Al_2O_3/water Nanofluid in Microchannel Heat Sink with Eulerian-Eulerian Approach

H. Hadi Najafabadi, M. Keshavarz Moraveji*

Department of Chemical Engineering, Amirkabir University of Technology (Tehran Polytechnic), Tehran, Iran.

ARTICLE INFO

Article history:
Received: 2016-02-07
Accepted: 2016-04-27

Keywords:
Nanofluid
Microchannel
Convective Heat Transfer
Friction Factor
Entropy Generation
CFD

ABSTRACT

In this paper, three-dimensional incompressible laminar fluid flow in a rectangular microchannel heat sink (MCHS) using Al_2O_3/water nanofluid as a cooling fluid is numerically studied. CFD prediction of fluid flow and forced convection heat transfer properties of nanofluid using single-phase and two-phase model (Eulerian-Eulerian approach) are compared. Hydraulic and thermal performance of microchannels are investigated according to the results of the friction factor, pumping power, average heat transfer coefficient, thermal resistance, average temperature of the walls and entropy generation. In addition, due to the CFD results, two correlations for prediction of Nusselt number and friction factor are presented. Comparing the predicted Nusselt number using single-phase and two-phase models with experimental data shows that the two-phase model is more accurate than single-phase model. The results show that increasing the volume fraction of nanoparticles leads to increases in the heat transfer coefficient and reduces the heat sink wall temperature, but it results in the undesirable effect of increase in pumping power and total entropy generation.

1. Introduction

With the frequently increasing power of microprocessors and other microelectronic components, improved heat transfer in microchannels has become a critical issue. Due to the limited ability of heat transfer, conventional cooling fluids such as water, oil and ethylene glycol cannot meet high cooling requirements [1]. So to overcome the increasing rate of heat recovery, new and effective methods should be introduced. Improved thermal conductivity is an effective way to increase heat transfer performance of conventional fluids. Choi and Eastman [2] proposed the use of nano-sized particles (smaller than 100 nm) to improve the conductivity of common fluids and termed the resulting mixture ‘‘nanofluid’’. Compared with suspension, with millimeter and micrometer

*Corresponding author: moraveji@aut.ac.ir

sized particles, nanofluids showed longer stability and less pressure drop [3].Various experimental and numerical studies have been carried out in order to investigate the effect of nanofluids in microchannel. Jung et al. [4] experimentally studied the convective heat transfer coefficient and friction factor of nanofluids in rectangular microchannels. The results showed that the heat transfer coefficient of Al_2O_3 nanofluid with volume fraction of 1.8 % increased 32 % compared to pure water in laminar flow regime. Ahmed et al. [3] investigated convective heat transfer in a rectangular microchannel heat sink with Lattice-Boltzmann method. The importance of external forces such as gravity, thermophoresis and Brownian forces have been considered in this study. The results suggest that in laminar region, Brownian forces have a significant effect on flow and heat transfer properties in low ranges of Reynolds numbers (Re ~ 1-10), but the effect of thermophoresis can be ignored for all flow conditions. Yang et al. [5] simulated flow and heat transfer of copper oxide / water nanofluid in a trapezoidal microchannel heat sink. Comparison of thermal resistance of single-phase and two-phase (mixture model) models and the experimental results indicated that the two-phase model is more accurate than single-phase model. In laminar flow, thermal resistance of nanofluid is less than water and its magnitude increases by increasing volume fraction of nanoparticles and volumetric flow rate. In addition, pressure drop increases slightly in the case of using nanofluid compared to pure water.

Entropy generation rate is the measurement of magnitude irreversibility during a process. According to the extent of entropy generation, the process efficiency can be determined [6]. Bejan [7] obtained entropy generation equations for forced convection heat transfer for different geometries. He found out that entropy generation rate in a system is the result of two contributions, thermal and frictional entropy generation rate. Thermal entropy generation occurs due to temperature difference between channel wall and fluid, while viscous or turbulent losses lead to frictional entropy generation [8]. Mehrali et al. [9] studied heat transfer characteristics and entropy generation for a graphene nano-platelet (GNP) nanofluid under laminar forced convection conditions inside a circular tube subjected to constant wall heat flux. In their experiments they concluded that by increasing nanoparticle concentration in a constant velocity flow, frictional entropy generation increases, while thermal entropy generation decreases. Also, total entropy generation had the same trend as thermal entropy generation. Hassan et al. [10] investigated the entropy generation of alumina/water nanofluid under laminar flow regime in minichannels and microchannels numerically. They found it more advantageous to use nanofluid in minichannel rather than microchannel.

The aim of this study is to compare single-phase and two-phase models to investigate the fluid flow and heat transfer characteristics of alumina/water nanofluid in a microchannel heat sink with a constant wall heat flux. Predictions are validated with referenced experimental data [11]. Various parameters such as pumping power, average microchannel wall temperature, thermal resistance, convective heat transfer coefficient and entropy generation are studied in order to

evaluate the performance of micro-channel heat sink. Also, the correlations for Nusselt number and friction factor are obtained based on CFD results.

2. Mathematical modeling

2.1. Geometry and grid

Geometry of rectangular microchannel and coordinate system used in this study is shown in Fig. 1. Also, dimensions of heat sink are summarized in Table 1. Cooling water passes through 25 parallel rectangular microchannels. All microchannels are assumed to have identical fluid flow and thermal properties. Therefore modeling and calculation were performed for a single channel.

To evaluate the independency of the results from the number of grid points used, a grid independency study is done considering the average error of Nusselt number calculated from experimental data [11]. For this study, a different number of grid points in the direction of x, y and z is used. According to the study, the number of grid points in the direction of x, y and z is15, 30 and 70 respectively.

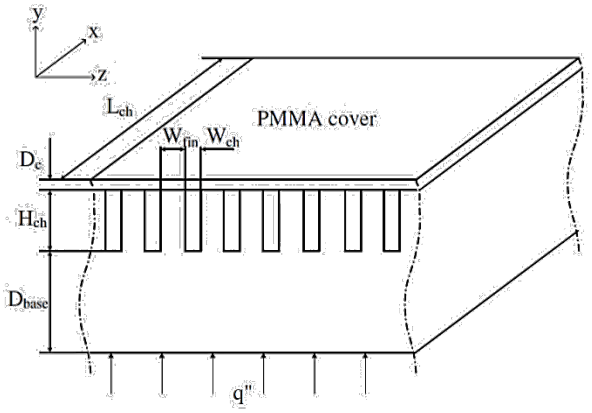

Figure 1. Geometry of rectangular microchannel heat sink.

2.2. Single-phase model

Single-phase model is used frequently to reduce the calculations and compare the results with the two-phase. In this model, the base fluid and particles are considered as a homogeneous phase and average properties are defined for nanofluid. The governing equations used for single-phase model are as follows:

Continuity equation:

$$\nabla.\left(\rho_{nf}.V_m\right)=0 \quad (1)$$

Momentum equation:

$$\nabla.(\rho_{nf}V_mV_m)=-\nabla P+\nabla.(\mu_{nf}.\nabla V_m) \quad (2)$$

Energy balance for coolant:

$$\nabla.(\rho_{nf}.C_p.V_m.T)=\nabla.(k_{nf}.\nabla T) \quad (3)$$

Conduction from solid wall:

$$0=\nabla.(k_w.\nabla T_w) \quad (4)$$

No slip condition on solid walls:

$$\vec{V}=0(@\text{Walls}) \quad (5)$$

Inlet and outlet conditions for microchannel:

$$\vec{V}=V_m(@\text{inlet}) \quad (6)$$

Table 1
Dimensions of microchannel heat sink.

$D_c\,(\mu m)$	$D_{base}\,(mm)$	$H_{ch}\,(\mu m)$	$L_{ch}\,(mm)$	$W_{ch}\,(\mu m)$	$W_{fin}\,(\mu m)$
10	24	800	50	283	300

$$P = \text{atmospheric pressure}(@\text{outlet}) \quad (7)$$

The upper wall of microchannel is assumed to be thermally insulated, while the bottom and side walls are exposed to constant heat flux:

$$-k_{nf}.\nabla T = q(@Bottom, left, right) \quad (8)$$

$$-k_{nf}.\nabla T = 0(@Top) \quad (9)$$

2.2.1. Thermo physical properties used in single-phase model

Thermo physical properties of alumina / water nanofluid, such as density, specific heat, thermal conductivity and viscosity, have been calculated according to the following equations:

Density:

$$\rho_{nf} = (1-\phi)\rho_{bf} + \phi\rho_{np} \quad (10)$$

Thermal conductivity:

$$\frac{k_{nf}}{k_{bf}} = \frac{2 + (k_{np}/k_{bf}) + 2\phi[(k_{np}/k_{bf}) - 1]}{2 + (k_{np}/k_{bf}) - \phi[(k_{np}/k_{bf}) - 1]} \quad (11)$$

Specific heat:

$$C_{p,nf} = \frac{1}{\rho_{nf}}[(1-\phi)\rho_{bf}C_{p,bf} + \phi\rho_{nf}C_{p,np}] \quad (12)$$

Viscosity:

$$\mu_{nf} = \frac{1}{(1-\phi)^{2.5}}\mu_{bf} \quad (13)$$

Thermo physical properties of nanoparticles (alumina), base fluid (water), and nanofluid alumina/water with volume fractions of 1 % and 2 % at $30^{\circ}C$ are given in Table 3. The calculated values show a significant increase in density and thermal conductivity of nanofluid compared with pure water.

Table 2

Grid independency study for pure water and Re=1500.

Case	Grid	Average of error % Nu from experimental
1	10×20×45	11.2
2	15×30×70	6.8
3	30×40×90	6.8

Table 3

Thermo physical properties of nanoparticles, base fluid and nanofluid at $40^{\circ}C$.

Properties	Nano-particle (alumina)	Base fluid (water)	Nanofluid (alumina-water) Φ=1 vol. %	Nanofluid (alumina-water) 2 vol. %
ρ (kg/m^3)	3600	995.1	1021.1	1047.2
$C_p(kJ/kgK)$	0.765	4.178	4.058	3.943
k (W/m K)	36.0	0.62	0.635	0.654
$\mu\times10^3$ (Ns/m^2)		0.7690	0.8062	0.9689

2.3. Eulerian-Eulerian model

In the Eulerian model different coupling methods can be employed between phases. Pressure is shared among all the phases, while the equations of continuity, momentum and energy for the primary and secondary phases are solved separately [12]:

- Volumetric conservation equation:

$$\sum_{q=1}^{n} \phi_q = 1 \quad (14)$$

- Continuity equation:

$$\nabla.(\phi_q\rho_q\vec{V}_q) = 0 \quad (15)$$

where $\vec{V}_q = \int_v \phi_q dV$ and $\sum_{q=1}^{n} \phi_q = 1$ and q represent the phase.

- Conservation of momentum (q^{th} phase)

$$\nabla.(\phi_q\rho_q\vec{V}\vec{V}) = -\phi_q\nabla P + \phi_q\nabla.(\mu_q\nabla\vec{V} + \sum_{k=1}^{n}\phi_k\rho_k\overline{v_k v_k}) + \phi_q\rho_q\vec{g} + \sum_{p=1}^{n}\vec{R}_{pq} \quad (16)$$

Where $\sum_{p=1}^{n}\vec{R}_{pq} = \sum_{p=1}^{n}S_{pq}(\vec{V}_p = \vec{V}_q)$ indicates interaction forces between the phases and $S_{pq} = (\phi_q\phi_p\rho_q\lambda)/\tau_p$, $\tau_p = (\rho_p d_p^2)/(18\mu_q)$. f is drag friction which is obtained as follows [13]:

$$\lambda = \frac{C_D.Re}{24} \quad (17)$$

$$C_D = \begin{cases}\dfrac{24(1+0.15Re^{0.687})}{Re}, & Re \le 1000\\ 0.44, & Re > 1000\end{cases} \quad (18)$$

$$Re = \frac{\rho_p|\vec{V}_p - \vec{V}_q|}{\mu_q} \quad (19)$$

Although Eqs (17) to (19) are originally used for macro scale particles, in some studies they have been applied for nanoparticles and concluded to satisfactory results [14-16]

Due to very small size of nanoparticles lift force contribution is negligible and is ignored in the current study [17].

- Conservation of energy:

$$\nabla.(\phi_q\rho_q\vec{V}_q H_q) = -\nabla.(k_q\nabla.T_q) - \tau_{q_t}:\nabla\vec{V}_q + \sum_{p=1}^{n}\vec{Q}_{pq} \quad (20)$$

where $\vec{Q}_{pq} = h(\vec{V}_p - \vec{V}_q)$ and the heat transfer coefficient is $h = \frac{6k_q\phi_q Nu_p}{d_p^2}$. Nu_p is calculated from [18]:

$$Nu_p = 2 + 0.6Re^{0.5}\mathrm{Pr}_p^{0.333} \quad (21)$$

2.4. Numerical solution

The governing equations are discretized using finite volume method. The algebraic equations resulted from discretization of governing equation are solved by using SIMPLE algorithm [19]. This algorithm is an iterative method whose calculation begins with an initial guess for flow field. Then momentum equation is solved to calculate the components of velocity profile. Pressure is corrected according to continuity equation. Although the continuity equation does not include pressure term, it can be converted to a pressure correction equation [20]. Repeating calculations continues to achieve negligible residual amounts (less than 10^{-7}).

3. Modeling validation

In order to validate this study, the results have been compared with experimental data from Ho et al. [11]. Figure 2 shows friction factor versus Reynolds number in the cases of pure water, volume fraction of 1 % and 2 % of alumina nanoparticles. According to this figure, in Re> 500, CFD and experimental friction factors deviate from the value 16/Re probably because the fluid's turbulency slightly increases. Table 4 also represents the deviation of the numerical results from experimental data. For example, the maximum deviation of the experimental data is equivalent to -16.68 % which occurred at volume fraction of 1 % and Reynolds number 1342.

Figure 3 shows Nusselt number versus Reynolds number for pure water, volume fraction of 1 % and 2 % of alumina nanoparticles in the case of single-phase and two-phase modeling. Also, Table 5 represents the deviation of the numerical results from experimental data. For example, in single-phase modeling maximum deviation from

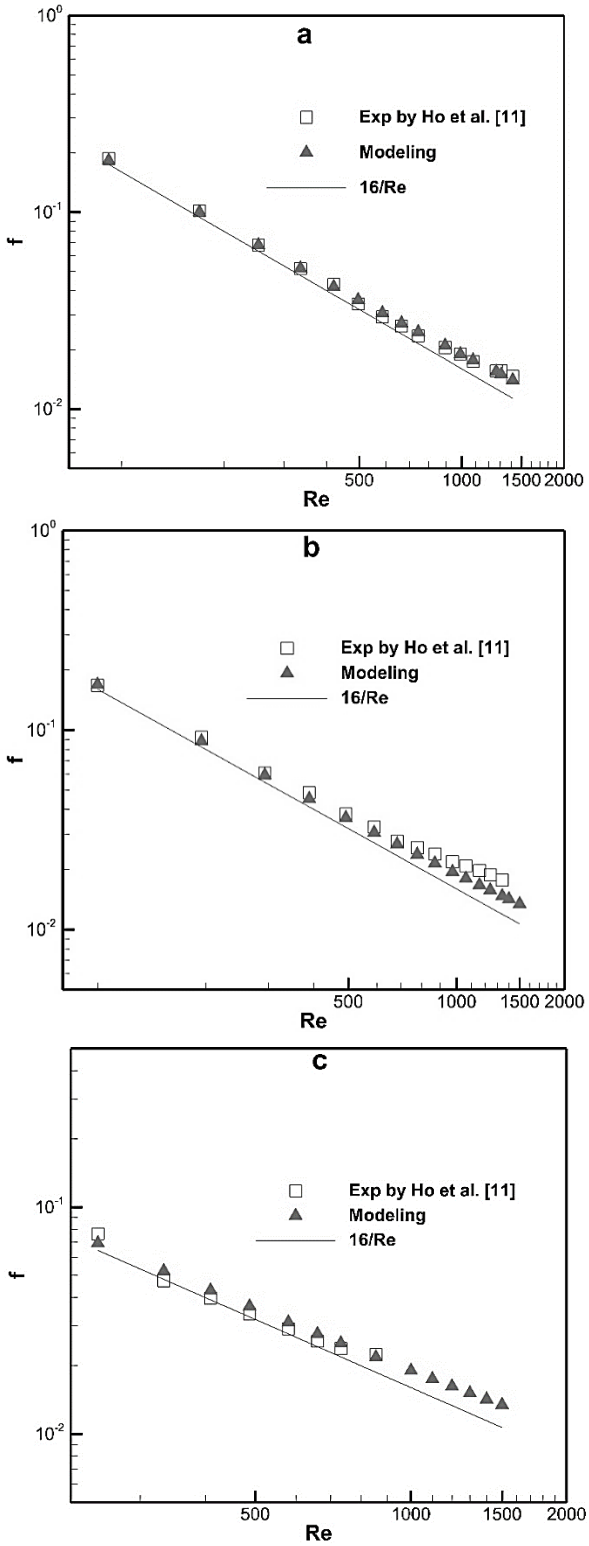

Figure 2. Modeling and experimental friction factor versus Reynolds number for a) pure water b) 1 % Alumina volume fraction c) 2 % Alumina volume fraction.

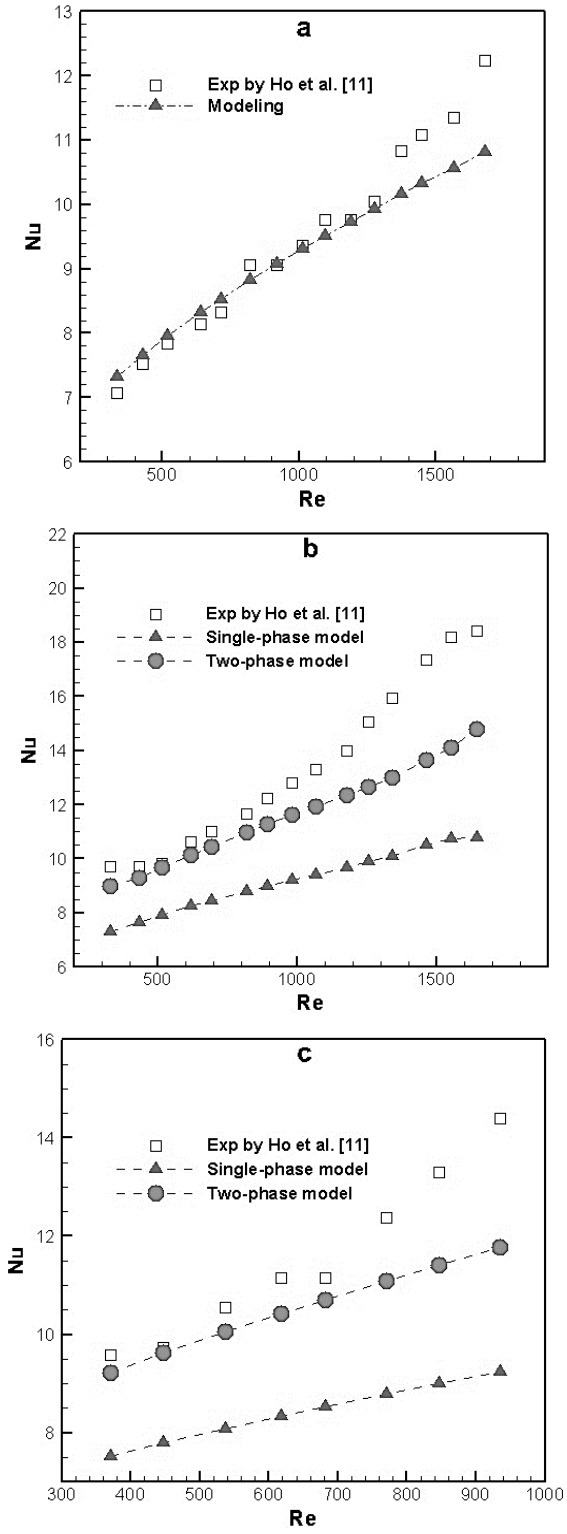

Figure 3. Single-phase and two-phase modeling and experimental friction factor versus Reynolds number for a) pure water b) 1 % Alumina volume fraction c) 2 % Alumina volume fraction.

Table 4
Deviation of friction factor numerical results from experimental data [11].

	min error %	max error %	Concentration (vol. %)	average error %
Magnitude	0.09	-16.68	0	0.53
at Reynolds	991	1342	1	-8.38
at volume fraction	0	1	2	4.45

Table 5
Deviation of Nusselt number numerical results from experimental data [11].

	min error %		max error %		Concentration (vol. %)	average error %	
	Single phase	Two phase	Single phase	Two phase		Single phase	Two phase
magnitude	0.16	-1.15	-41.48	-22.38	0	-1.80	
at Reynolds	919	448	1647	1554	1	-29.52	-11.07
at volume fraction	0	2	1	1	2	-26.33	-7.90

experimental data is 41.48 % for Reynolds number 1647 and volume fraction 1 %, while in two-phase modeling the maximum deviation from experimental data is 22.38 % for Reynolds number 1554 and volume fraction 1 %. Comparing average errors of simulation results, it is concluded that two-phase model is less deviated from experimental data.

4. Results and discussion

Figure 4 (a and b) shows the contour of the microchannel heat sink temperature for Re=336, Φ = 0 and Re = 1500, Φ = 0.02. Numerical modeling results indicate that temperature increases along the channel in the direction of fluid flow. In addition, the increase in Reynolds number and volume fraction of Alumina nanoparticles decreases the average temperature of the walls and fluid.

4.1. Heat transfer correlation

Average Nusselt number is obtained using the following equation:

$$\overline{Nu} = \frac{\bar{h} D_h}{k_{nf}} \tag{22}$$

where D_h is hydrodynamic diameter. It is calculated by:

$$D_h = \frac{4 W_{ch} H_{ch}}{2(W_{ch} + H_{ch})} \tag{23}$$

In Eq. (22) $\bar{h}$ is average convective heat transfer coefficient which is evaluated by:

$$\bar{h} = \frac{q_{in}}{A_b (T_{w,avg} - T_{f,avg})} \tag{24}$$

where $T_{w,avg}$ and $T_{f,avg}$ are average wall temperature and average fluid temperature, respectively. These parameters are calculated using Eq. (25) and (26):

$$T_{w,avg} = \frac{1}{A_b} \int T_w dA \tag{25}$$

$$T_{f,avg} = \frac{\int T_f \rho \left| \vec{v}. d\vec{A} \right|}{\int \rho \left| \vec{v}. d\vec{A} \right|} \tag{26}$$

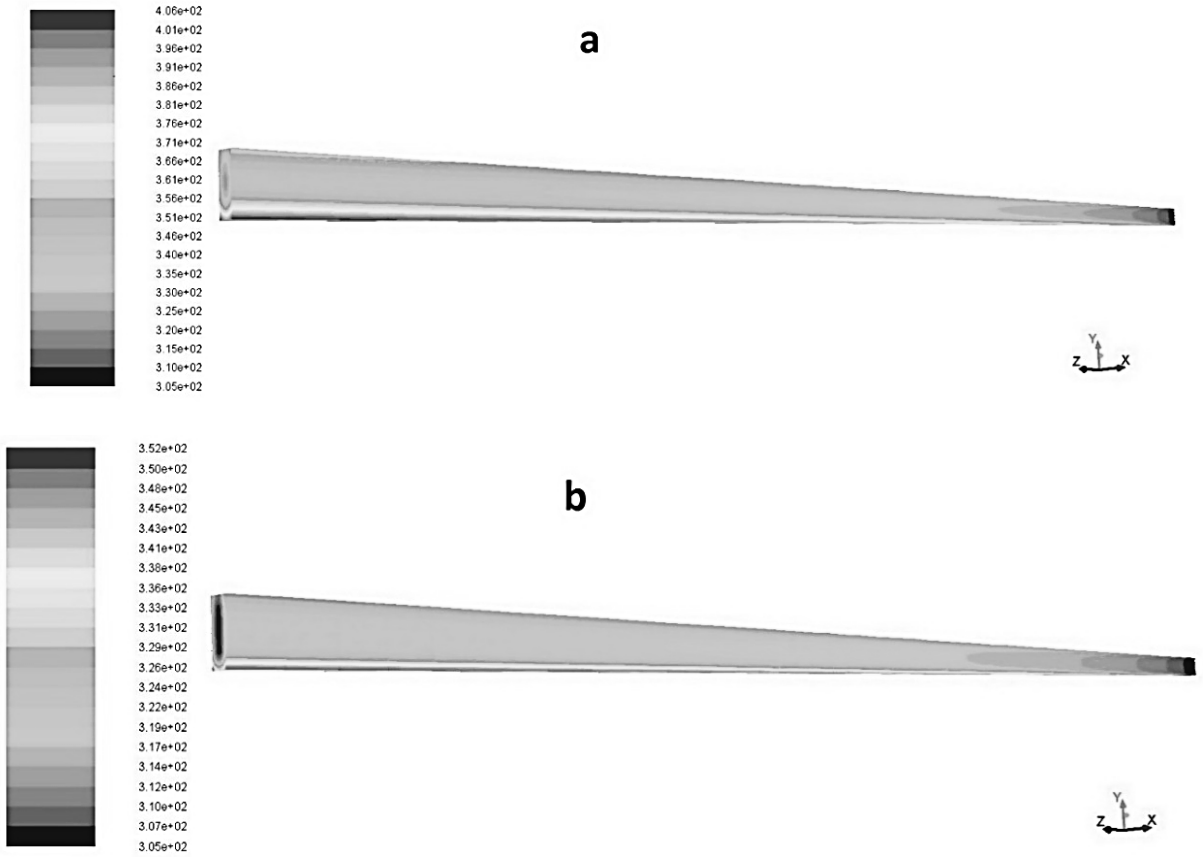

Figure 4. The contours of temperature (K) in microchannel heat sink for a) Re=336,Φ=0 b) Re=1500,Φ=0.02.

A_b is the area of the wall that heat flux is applied to:

$$A_b = NL_{ch}(W_{ch} + 2H_{ch}) \quad (27)$$

Nusselt number is defined as the ratio of convective to conductive heat transfer and for laminar flow regime of nanofluid in a microchannel heat sink is obtained from the following equation [21]:

$$Nu = 0.28\mathrm{Re}^{0.35}\mathrm{Pr}^{0.36} \quad (28)$$

According to Eq. (28), Nusselt number depends on different parameters such as thermal conductivity, heat capacity, density and velocity. Considering the results of the present modeling, Nusselt number in a microchannel heat sink can be correlated as a function of Reynolds number, Prandtl number and the volume fraction of particles:

$$Nu = 0.35\mathrm{Re}^{0.4}\mathrm{Pr}^{0.43}(1+\phi)^{9.8}$$
$$226 < \mathrm{Re} < 1676, 4.16 < \mathrm{Pr} < 4.79 \quad (29)$$

Reynolds and Prandtl numbers are defined as follows:

$$Re = \frac{u_m . D_h . \rho}{\mu} \quad (30)$$

$$\mathrm{Pr} = \left(\frac{C_p \mu}{k}\right)_{nf} \quad (31)$$

Figure 5 represents correlated Nusselt number versus Nusselt number calculated from modeling results. The highest, lowest and average errors of modeling Nusselt number from correlated ones are 17.6 %, 0.07 % and 2.1 %, respectively.

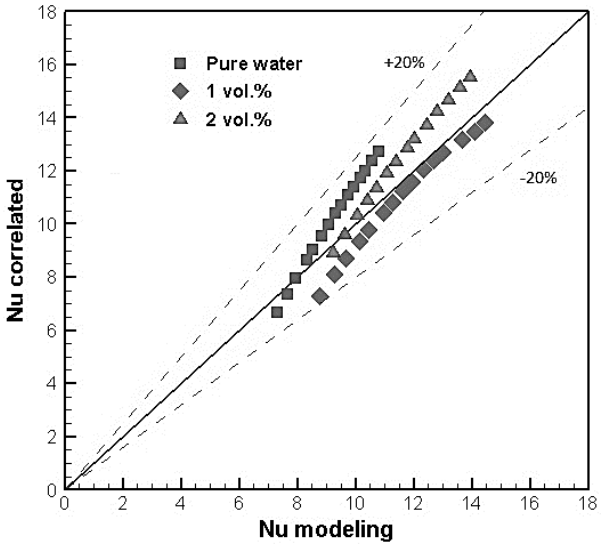

Figure 5. Comparison between correlated Nusselt number versus modeling ones.

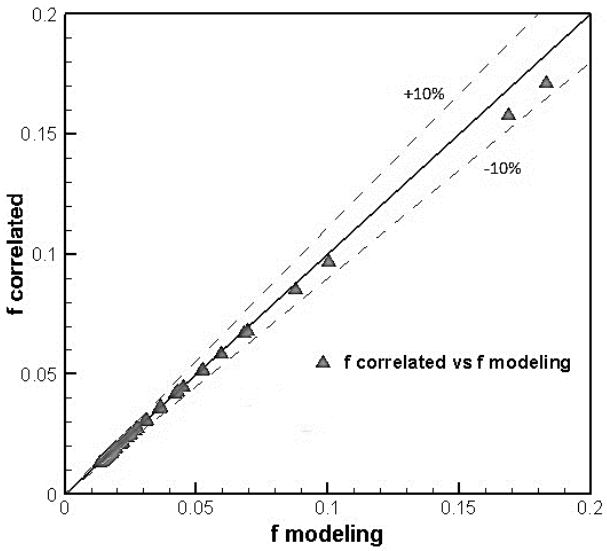

Figure 6. Comparison between correlated Fanning friction factor versus modeling ones.

4.2. Friction factor correlation

Fanning friction factor in a heat sink is obtained using Hagen-Poiseuille equation:

$$f = \frac{\Delta p . D_h}{2\rho_{nf} u_m^2 L_{ch}} \quad (32)$$

For present modeling, Eq. (32) for friction factor is correlated by considering the effect of volume fraction of nanoparticles:

$$f = 11.373\mathrm{Re}^{-0.929}(1+\phi)^{4.8}$$
$$226 < \mathrm{Re} < 1676 \quad (33)$$

Error of this correlation is about 10 %. Figure 6 shows the friction factor correlated versus the friction factor calculated from modeling results. According to the figure there is a relatively good match between correlated and modeling friction factor.

4.3. Pumping power

When the cooling fluid passes through the narrow channel heat sink, pressure drop occurs. To overcome this pressure drop, the system will need extra pumping power. Pumping power can be approximated using Eq. (34):

$$P_p = \dot{Q} . \Delta P \quad (34)$$

Figure 7 represents variation of pumping power versus volumetric flow rate and volume fraction of Alumina nanoparticles. Higher density of nanofluid compared with pure water is the main reason of pumping power increase

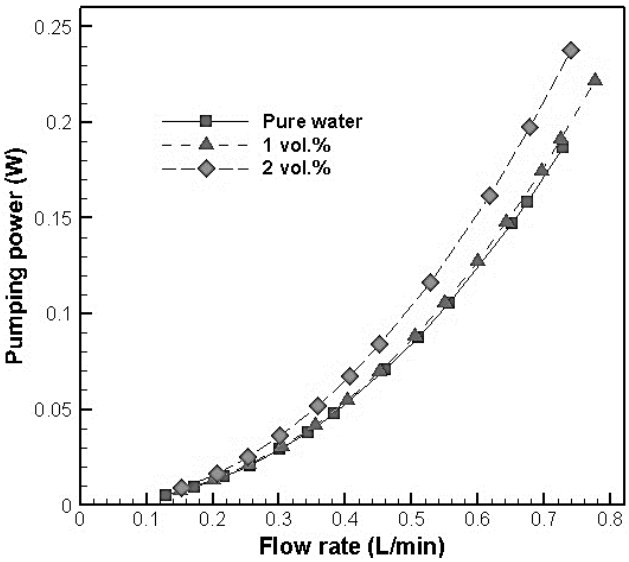

Fig. 7. Variation of pumping power versus volumetric flow rate and volume fraction of nanoparticles.

in the case of using nanofluid. Another reason is the increased viscosity of nanofluid. But this extra pumping power may be compensated considering the improvement in efficiency of nanofluid compared with pure water.

4.4. Average temperature difference

Equation (24) shows that there is an inverse relationship between convective heat transfer coefficient and the average temperature difference. Convective heat transfer coefficient is also highly dependent on other thermal properties. Changes in average temperature difference between the fluid and the wall by changing the Reynolds number and volume fraction of nanoparticles in the case of single-phase and two-phase models are shown in Fig. 8. Increasing the volume fraction of nanoparticles and Reynolds number leads to a decrease in the average temperature difference. In addition, it is seen that two-phase model predicts a greater reduction in average temperature difference compared with single-phase model. Maximum reduction in average temperature difference is equivalent to 25.1 % compared with pure water which occurs at the highest Reynolds number (1500) and for nanofluid with volume fraction of 2 %. Increasing Reynolds number reduces the temperature difference.

4.5. Average heat sink base temperature

The main purpose of a cooling system is to reduce wall temperature of the walls and thus the heat source temperature, and maintain it at a certain amount. The use of nanofluid with different volume fraction in the Reynolds range of 331 to 1678 is shown in Fig. 9.

As seen in Fig. 9 increase in volume fraction of nanoparticles has a significant impact on reducing the average wall temperature of microchannel. Also, by increasing the Reynolds number, wall temperature can be

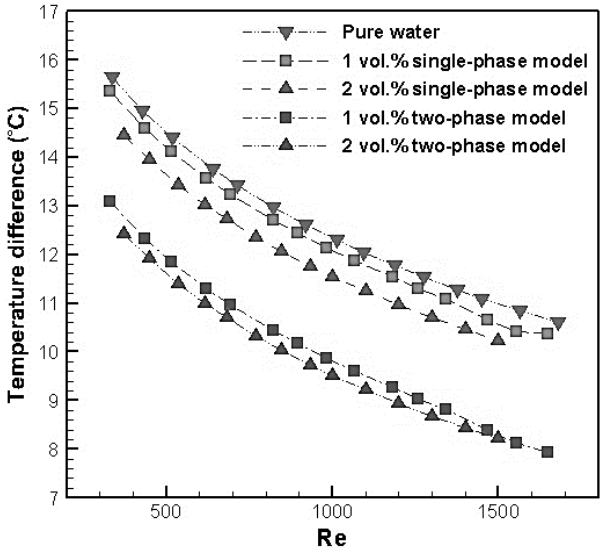

Figure 8. Variation of average temperature difference versus Reynolds number and volume fraction of Alumina nanoparticles.

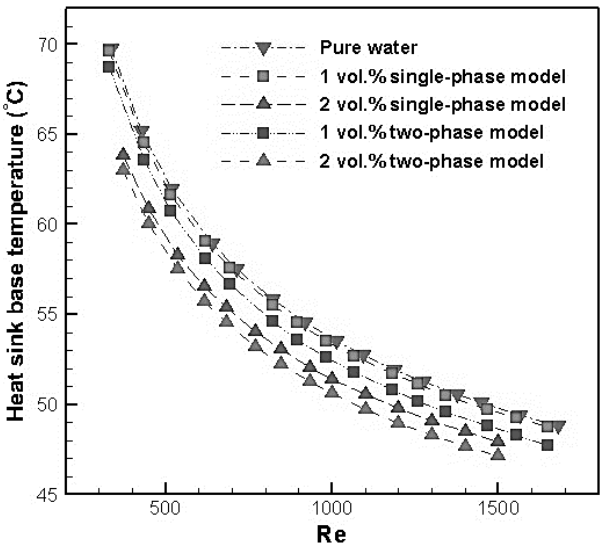

Figure 9. Effect of addition of Alumina nanoparticles and changing Reynolds number on heat sink base temperature.

minimized to the desired value. In this study, the maximum decrease in wall temperature is equivalent to 4.8°C compared with pure water which occurs at the lowest Reynolds number (336) for a volume fraction of 2 %, while increasing the Reynolds number will lessen the wall temperature decrease. According to the figure, it can be stated that nanofluid absorbs more heat compared with pure water. Also, addition of nanoparticles has increased heat absorption dramatically. Furthermore, two-phase model predicts more reduction in wall temperature compared with single-phase model.

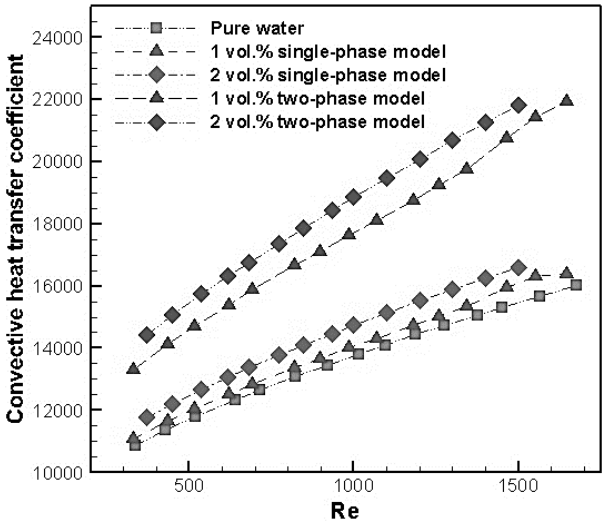

Figure 10. Variation of convective heat transfer coefficient versus Reynolds number.

4.6. Convective heat transfer coefficient

Thermal efficiency of nanofluid depends on the convective heat transfer coefficient. Effect of Reynolds number and volume fraction of alumina nanoparticles on convective heat transfer coefficient in the case of single-phase and two-phase modeling is shown in Fig. 10. Increase in the Reynolds number and volume fraction of nanoparticles has substantially improved the convective heat transfer coefficient. However, two-phase model predicts values greater than single-phase model, so that 28.9 % enhancement in heat transfer coefficient of nanofluid with a volume fraction of 2 % at Reynolds 1500 in comparison with pure water is predicted.

Adding nanoparticles to the base fluid increases thermal conductivity and Brownian motion, factors that directly improve the thermal performance of nanofluid compared with pure water. The Reynolds number increase represents enhancement in heat capacity of cooling fluid which maximizes the reduction of microchannel base temperature.

4.7. Thermal resistance

Convective thermal resistance has significant effects on the efficiency of thermal cooling. Convective thermal resistance for a cooling fluid can be calculated using the following equation:

$$R_{th} = \frac{1}{\bar{h}A_b} = \frac{T_{w,avg} - T_{f,avg}}{q_{in}} \qquad (35)$$

Figure 11 shows variation of heat transfer resistance versus Reynolds number at different volume fractions of alumina nanoparticles. As seen in the figure the thermal resistance decreases with increasing Reynolds number. Also, increase in the volume of nanoparticles will lead to lower thermal resistance. Adding nanoparticles increases the heat transfer coefficient and thermal mixing that are the main factors responsible for reducing the convective thermal resistance compared to the base fluid.

It is observed in Fig. 11 that two phase modeling suggests a greater reduction of thermal resistance than single phase modeling. In this modeling maximum reduction in

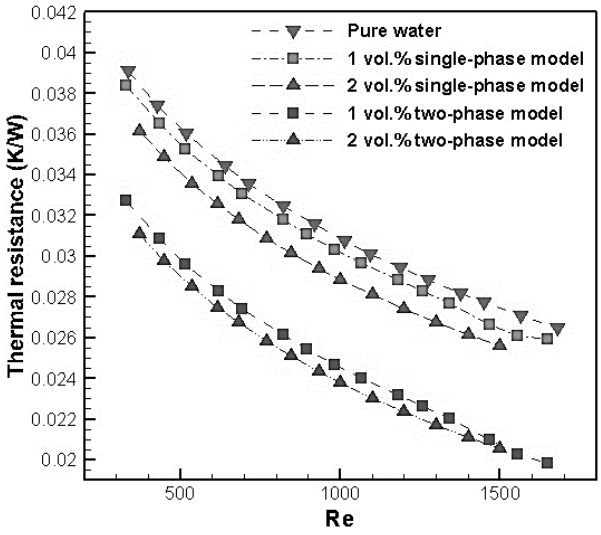

Figure 11. Variation of thermal resistance versus Reynolds number at different volume fractions of Alumina nanoparticles.

thermal resistance is equivalent to 23.7 % compared to the pure water which occurs in a volume fraction of 2 % and at the highest Reynolds number (1500). At high Reynolds numbers, Brownian motion of particles increases due to high velocity of nanofluid, resulting in increasing the heat transfer. Heat transfer enhancement increases heat transfer coefficient which has an inverse relationship with thermal resistance. Thus increasing the convective heat transfer coefficient will reduce the convective thermal resistance.

4.8. Entropy generation rate

Entropy generation rate for the considered configuration is obtained in two parts [22, 23]:

$$S_{gen,T} = S_{gen,t} + S_{gen,f} \quad (36)$$

The two contributions represent the thermal irreversibility and flow frictional losses. In order to examine the effect of each contribution to the total entropy generation rate, a dimensionless parameter, the Bejan number (Be), is considered:

$$Be = \frac{S_{gen,t}}{S_{gen,T}} \quad (37)$$

The value of Bejan ranges from 0 to 1. Accordingly, Be = 0 and Be = 1 are two limiting cases where the irreversibility is controlled by fluid friction and heat transfer, respectively.

The two contributions expressed in Eq. (37) can be expressed in a more convenient form [22] as:

$$S'_{gen,T}(x) = \frac{q'.\Delta T(x)}{T^2} + \frac{\dot{m}}{\rho.T}\left(-\frac{dp}{dx}\right) \quad (38)$$

Eq. (38) represents the local total entropy generation per unit length. In this equation the first term represents thermal entropy generation and the second is the frictional entropy generation.

Integrating Eq. (38), the following expression is obtained[22]:

$$S_{gen,T} = \frac{q^2.A_b.D_h}{Nu.k_{nf}.T_{avg}^2} + \frac{2\dot{m}^3.f.L_{ch}}{\rho_{nf}^2.T_{avg}.D_h.A_c^2} \quad (39)$$

Therefore, thermal and frictional entropy generation rates are calculated with the following equations:

$$S_{gen,t} = \frac{q^2.A_b.D_h}{Nu.k_{nf}.T_{avg}^2} \quad (40a)$$

$$S_{gen,f} = \frac{2\dot{m}^3.f.L_{ch}}{\rho_{nf}^2.T_{avg}.D_h.A_c^2} \quad (40b)$$

Figure 12 represents changes in thermal and frictional entropy generation rate because of the variation of Reynolds number as well as volume fraction of nanofluid. According to the figure, frictional entropy generation rate increases with the Reynolds number. Although increasing the Reynolds number reduces the friction factor and the average temperature in Eq. (40b), increasing the mass flow rate passes

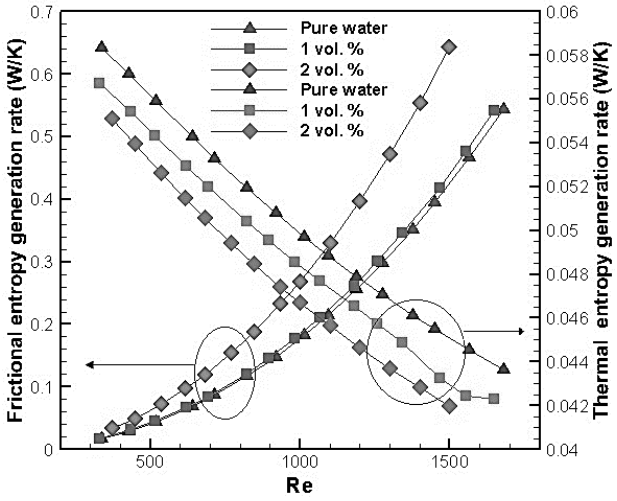

Figure 12. Frictional and thermal entropy generation vs. Reynolds number for different volume fractions of nanoparticles.

over them. Also, adding nanoparticles increases the frictional entropy generation rate that can be caused by the reduction of average temperature and rise of friction factor compared with pure water.

Thermal entropy generation rate increases with increasing Reynolds number. Also, adding nanoparticles to the base fluid decreases thermal entropy generation rate due to increase in Nusselt number and thermal conductivity in Eq. (40a). Frictional entropy generation rate prevails over thermal entropy production rate in the main range of Reynolds numbers. This can be caused by significant effect of small size of microchannel. That is why the total entropy generation rate will be similar to the rate of frictional entropy generation. So to reduce the irreversibility using nanofluid with low volume fractions and at low Reynolds numbers ranges is recommended. Although this recommendation has a positive effect in reducing the pumping power (Fig. 7), it should also be considered that according to Figs. 10 and 11, decreasing flow rate and volume fraction of nanoparticles reduces heat transfer enhancement compared to pure water. So the impact of these factors must be considered in finding optimum volumetric flow rate and volume fraction of nanoparticles.

The Bejan number is the ratio of heat transfer irreversibility to total irreversibility due to heat transfer and fluid friction. Figure 13 shows changes in Bejan number with the variation of Reynolds number and volume fraction of nanoparticles. Bejan number decreases with increasing Reynolds number and adding nanoparticles. In other words, increasing the volumetric flow rate of fluid and adding nanoparticles leads to reduction in thermal entropy generation rate contribution, so that for Reynolds numbers greater than 1000 the thermal entropy generation rate contribution for nanofluid with 2 % volume fraction of Al_2O_3 reduces to less than 15 % .

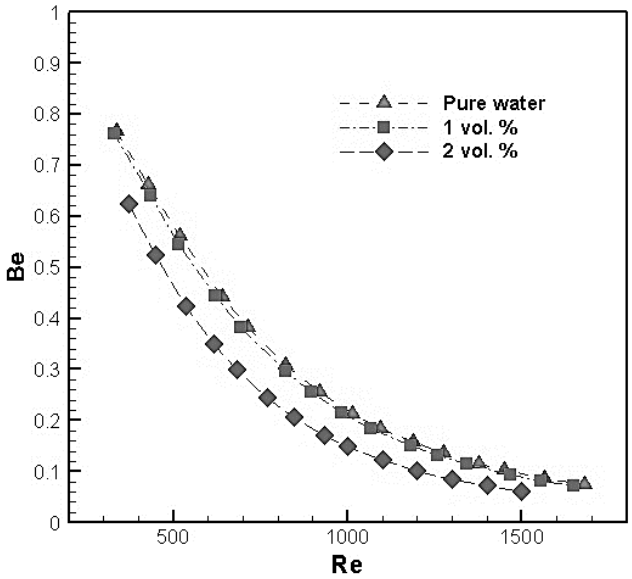

Fig. 13. Bejan number versus Reynolds number for different volume fractions of Alumina nanoparticles.

5. Conclusions

Laminar forced convection heat transfer in a rectangular microchannel heat sink with alumina/water nanofluid was investigated numerically. Finite volume method was used to discretize the governing equations. Nusselt number and friction factor predictions using single-phase and two-phase models were validated due to experimental data[11]. Nusselt number results indicate more accurate modeling of two-phase model compared with the single-phase model. Also, correlations for Nusselt number and friction factor were obtained according to the modeling results. The overall performance of nanofluid in microchannels was compared with pure water that led to the following conclusions:

• Significant enhancement in heat transfer coefficient (26 %) was obtained using nanofluid compared with pure water. Also, Nusselt number rose sharply with the increase of nanoparticles volume fraction and Reynolds number.

• Increasing the volume fraction of nanoparticles and Reynolds number minimized the convective thermal resistance.

• Due to the negligible amounts of thermal entropy generation, the total entropy generation presented similar changes to those of frictional entropy generation. In other words, total entropy generation rose by increasing the Reynolds number and nanoparticle volume fraction.

Increase in the volume fraction of nanoparticles and Reynolds number in microchannels had positive effects such as reducing thermal resistance, increasing the heat transfer coefficient and reduction of the heat sink wall temperature, but caused increased pumping power and entropy generation as unfavorable results.

Nomenclature

Be	Bejan number.
C_p	specific heat [$kJ.kg^{-1}.K^{-1}$].
D_h	hydraulic diameter [m].
H_{ch}	height of microchannel [μm].
H	Entropy [$J.K^{-1}$].
$\overline{h}$	average heat transfer coefficient [$W.m^{-2}.K^{-1}$].
f	friction factor.
k	thermal conductivity [$W.m^{-1}.K^{-1}$].
L_{ch}	length of microchanne [mm].
$\dot{m}$	mass flow rate [$kg.s^{-1}$].
N	number of microchannel.
$\overline{Nu}$	average Nusselt number.
ΔP	pressure drop [Pa].
Q'	volumetric flow rate [$cm^3.min^{-1}$].
q_{in}	total heating power [W].
q	heat flux [$W.m^{-2}$].
q´	heat transfer per unit of lengt [$W.m^{-1}$].
g	gravitational acceleration [$m.s^{-2}$].
Pr	Prandtl number.
Re	Reynolds number.
T	temperature [K].
V_m	mean velocity [$m.s^{-1}$].
W_{ch}	width of a unit microchannel [mm].
P_p	pumping power [W].
S_{gen}	entropy generation [$W.K^{-1}$].
S'_{gen}	entropy generation per unit of length [$W.K^{-1}.m^{-1}$].
R_{th}	thermal resistance [$K.W^{-1}$].
C_D	drag coefficient.
d_p	particle diameter [m].

Greek letters

μ	dynamic viscosity [$Pa.s$].
ρ	density [$kg.m^{-3}$].
ϕ	volume fraction of nanoparticles.
β	interphase drag coefficient[$Pa.s.m^{-1}$].
ι	shear stress [Pa].
γ	bulk viscosity [$Pa.s$].
λ	drag friction.

Subscripts

T	total.
t	thermal.
f	frictional.
bf	base fluid.
ch	microchannel.
nf	nanofluid.
w	wall.
avg	average.
np	nanoparticles.

References

[1] Zhang, H., Shao, S., Xu, H. and Tian, C., "Heat transfer and flow features of Al_2O_3–water nanofluids flowing through a circular microchannel : Experimental results and correlations", *App. Therm. Eng.*, **61**, 86 (2013).

[2] Chol, S., "Enhancing thermal conductivity of fluids with nanoparticles", *ASME-Pubs-Fed*, **231**, 99 (1995).

[3] Ahmed, M. and Eslamian, M., "Laminar forced convection of a nanofluid in a microchannel: Effect of flow inertia and external forces on heat transfer and fluid flow characteristics", *App. Therm. Eng.*, **78**, 326 (2015).

[4] Jung, J.Y., Oh, H.S., and Kwak, H.Y., "Forced convective heat transfer of nanofluids in microchannels", *Int. J. of Heat Mass Trans.*, **52**, 466 (2009).

[5] Yang, Y.T., Tsai, K.T., Wang, Y.H. and Lin, S.H., "Numerical study of microchannel heat sink performance using nanofluids", *Int. Commun. Heat Mass Trans.*, **57**, 27 (2014).

[6] Bejan, A., "Second law analysis in heat transfer", *Energy*, **5**, 720 (1980).

[7] Bejan, A., "General criterion for rating heat-exchanger performance", *Int. J. Heat Mass Trans.*, **21**, 655 (1978).

[8] Singh, P.K., Anoop, K., Sundararajan, T. and Das, S.K., "Entropy generation due to flow and heat transfer in nanofluids", *Int. J. Heat Mass Trans.*, **53**, 4757 (2010).

[9] Mehrali, M., Sadeghinezhad, E., Rosen, M.A., Akhiani, A.R., Latibari, S.T., Mehrali, M. and Metselaar, H.S.C., "Heat transfer and entropy generation for laminar forced convection flow of graphene nanoplatelets nanofluids in a horizontal tube", *Int. Commun. Heat Mass Trans.*, **66**, 23 (2015).

[10] Hassan, M., Sadri, R., Ahmadi, G., Dahari, M.B., Kazi, S.N., Safaei, M.R. and Sadeghinezhad, E., "Numerical study of entropy generation in a flowing nanofluid used in micro and minichannels", *Entropy*, **15**, 144 (2013).

[11] Ho, C.J., Wei, L.C., and Li, Z.W., "An experimental investigation of forced convective cooling performance of a microchannel heat sink with Al_2O_3/water nanofluid", *App. Therm. Eng.*, **30**, 96 (2010).

[12] Akbari, M., Galanis, N. and Behzadmehr, A., "Comparative assessment of single and two-phase models for numerical studies of nanofluid turbulent forced convection", *Int. J. Heat Fluid Flow*, **37**, 136 (2012).

[13] Schiller, L. and Naumann, A., "A drag coefficient correlation", *Vdi Zeitung*, **77**, 51 (1935).

[14] Kalteh, M., Abbassi, A., Saffar-Avval, M., and Harting, J., "Eulerian–Eulerian two-phase numerical simulation of nanofluid laminar forced convection in a microchannel", *Int. J. Heat Fluid Flow*, **32**, 107 (2011).

[15] Kalteh, M., "Investigating the effect of various nanoparticle and base liquid types on the nanofluids heat and fluid flow in a microchannel", *App. Math. Model.*, **37**, 8600 (2013).

[16] Salman, B.H., Mohammed, H.A., and Kherbeet, A.S., "Numerical study of three different approaches to simulate nanofluids flow and heat transfer in a microtube", *Heat Transfer—Asian Research*, **45**, 46 (2016).

[17] Fani, B., Kalteh, M., and Abbassi, A., "Investigating the effect of Brownian motion and viscous dissipation on the nanofluid heat transfer in a trapezoidal microchannel heat sink", *Adv. Powder Tech.*, **26**, 83 (2015).
[18] Ranz, W. and Marshall, W., "Evaporation from drops", *Chem. Eng. Prog.*, **48**, 141 (1952).
[19] Anderson, J.D., Computational fluid dynamic: The basics with applications, *McGraw-Hill, New York*, (1995).
[20] Patankar, S.V., Numerical heat transfer and fluid flow, *Hemisphere, New York*, (1980).
[21] Maiga, S.E.B., Palm, S.J., Nguyen, C.T., Roy, G. and Galanis, N., "Heat transfer enhancement by using nanofluids in forced convection flows", *Int. J. Heat Fluid Flow*, **26**, 530 (2005).
[22] Bejan, A., Entropy generation minimization: The method of thermodynamic optimization of finite-size systems and finite-time processes, *CRC Press*, (1995).
[23] Bianco, V., Manca, O. and Nardini, S., "Entropy generation analysis of turbulent convection flow of Al_2O_3–water nanofluid in a circular tube subjected to constant wall heat flux", *Energy Conv. Manag.*, **77**, 306 (2014).